AMERICAN SCIENTIFIC PUBLISHERS

Science of Advanced Materials
Vol. 11, pp. 756–763, 2019
www.aspbs.com/sam

ARTICLE

Component Determination and Their Formation of $PM_{2.5}$

Mei-Mei Wang[1], Yong-Jie Zheng[1,*], Tao Jing[1,*], Jing-Zhi Tian[1], Peng-Shan Chen[1], Meng-Yao Dong[2,3], Chao Wang[7], Chao Yan[4], Chuntai Liu[3,*], Tao Ding[5,*], Wei Xie[6,*], and Zhan-Hu Guo[2,*]

[1]*College of Chemistry and Chemical Engineering, Qiqihar University, Qiqihar 161006, China*
[2]*Integrated Composites Laboratory (ICL), Department of Chemical & Biomolecular Engineering, University of Tennessee Knoxville, TN 37934, USA*
[3]*National Engineering Research Center for Advanced Polymer Processing Technology, Zhengzhou University, Zhengzhou, 450002, China*
[4]*School of Material Science and Engineering, Jiangsu University of Science and Technology, Zhenjiang, Jiangsu, 212003, China*
[5]*College of Chemistry and Chemical Engineering, Henan University, Kaifeng, 475004, China*
[6]*Key Laboratory of Lightweight and Reliability Technology for Engineering Vehicle, The Education Department of Hunan Province, Changsha University of Science & Technology, Changsha 410114, China*
[7]*College of Materials Science and Engineering, North University of China, Taiyuan 030051, China*

ABSTRACT

Informatics analysis on inorganic compounds, surface imaging and depth profiling were carried out for $PM_{2.5}$ using time-of-flight secondary ion mass spectrometry (TOF-SIMS) during different haze periods (autumn and winter). Both positive ions, such as NH_4^+, Si^+, H^+, Li^+, Na^+, Mg^+, Al^+, K^+, Ca^+, Ti^+, Cr^+, Fe^+, Cu^+, As^+, Cs^+ and Ba^+, and negative ions, such as NO_2^-, NO_3^-, SO_3^{2-}, SO_4^{2-}, O^-, Cl^-, CN^- and H^-, were detected in the samples. Along with the increase of the depth, the signal intensity became weaker and weaker for most of the inorganic ions, however, it could be stronger for a few of them due to the variation of chemical behaviors. Moreover, the source analysis was performed, and the results indicated that $PM_{2.5}$ was mainly derived from biomass combustion and fossil combustion in this area. This paper is useful to provide a tool to study the $PM_{2.5}$ around the world.

KEYWORDS: $PM_{2.5}$, TOF-SIMS, Image, Depth Profiling.

1. INTRODUCTION

With the rapid development of materials science and technology, more and more materials are widely used in all walks of human's life,[1–10] but the problem of environmental pollution is becoming more and more serious, and it will become an important factor restricting human development. Environmental issues, such as over-harvesting, fuel leaks, water pollution, and dust will have a serious impact on human living environment and industrial production.[11–22] To find a balance between the development and environmental protection is the focus of people's attention. Among the many environmental problems, haze is no longer a new topic, but it is still the focus of public attention because $PM_{2.5}$ in haze can cause respiratory diseases, Cardio-Cerebral-Vascular diseases, and other diseases easily,[23–29] and undoubtedly influence both growing development and physique of children and adolescents.[29] To study this in more focused way, we focus on the north part of China where the energy was supplied by consuming coal and other fossil-based fuels. For example, Qiqihar is located in Songnen plain, one of three major black soil regions of the world, and is the important base for green food production in China. Therefore, it is of great significance to carry out monitoring and researching $PM_{2.5}$ in order to control the air pollution and protect the environment effectively in Qiqihar area.

However, it is a challenging task because there are many air pollution sources, and each of them consists of complex organic and inorganic compounds. It is necessary to analyze the chemical components of $PM_{2.5}$ in haze because the chemical compositions and interactions among these compositions certainly play a dominant role in determining the aerosol behavior and characteristics.[30–32]

*Authors to whom correspondence should be addressed.
Emails: zyj1964@163.com, jtkr@163.com, ctliu@zzu.edu.cn, dingtao@henu.edu.cn, xwxw00@163.com, zguo10@utk.edu
Received: 16 July 2018
Accepted: 20 September 2018

There are many ways to characterize the organic and inorganic compounds, such as X-ray photoelectron spectroscopy (XPS), scanning electron microscopy-energy dispersive X-ray spectroscopy (SEM-EDS), X-ray powder diffraction (XRD), and time-of-flight secondary ion mass spectrometry (TOF-SIMS),[33–38] in which TOF-SIMS is one of the important research tools,[39–43] because more convincing results can be obtained than other analytical techniques in the identification of compounds. Currently, TOF-SIMS has been applied to many fields including surface characteristics of aerosol particles, the depth distribution characteristics of chemical composition, surface chemical reactions, chemical toxicity, and emission characteristics of pollution sources. Different work patterns of TOF-SIMS can be applied to different aspects of aerosol analysis.[44] Static TOF-SIMS is mainly used for surface analysis and surface imaging of $PM_{2.5}$. Dynamic TOF-SIMS is mainly applied for depth profiling and three-dimensional imaging of $PM_{2.5}$. In addition, it is easy to use TOF-SIMS to obtain information regarding $PM_{2.5}$, including various inorganic and organic compounds.

In this study, the inorganic compositions and distributions for $PM_{2.5}$ were characterized by TOF-SIMS, the depth profiling was performed for the core of the particles, the chemical behaviors were analyzed, and the sources of the particles were addressed. Our results provide a basis for government decision making on environmental improvement.

2. EXPERIMENTAL DETAILS

2.1. Study Area and Sampling

The study area was Qiqihar shown in Figure 1, which was located in the Songnen Plain in the north of China (123.57°E, 47.23°N) and covered an area of 442 87 km^2. The samples of airborne $PM_{2.5}$ were collected at chemical laboratory center of the Qiqihar University in November and December. The sampling time was from 8:30 am to 8:30 am next morning, 24 h each day. The Intelligent Atmospheric Sampler (Tianhong Inc., China) was applied for sample collections with a flow rate of 16.7 L/min. The quartz filter (Munktell) having a diameter of 47 mm with pore size of 0.3 μm was used.

Before sampling, the quartz filter wrapped by tin foil had been oven-baked at 400 ± 10 °C for 5 h in a muffle furnace to eliminate the influence of the membrane component on the analysis. The membranes were maintained in a chamber with temperature (25 ± 2 °C) and a relative humidity ($40 \pm 5\%$) for 48 h before and after sampling. All filters were weighed with an analytical balance (Sartorius, Germany) at least three times before and after sampling, following the 48 h equilibration period. The samples after sampling were put in a clean packaging bag and protected from light in a refrigerator (−4 °C) until composition analysis.

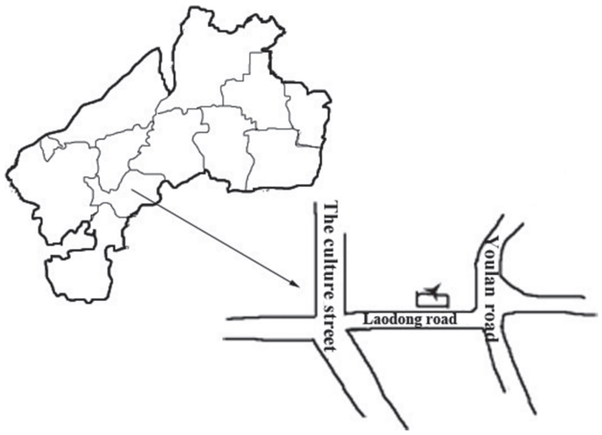

Fig. 1. Sampling location of $PM_{2.5}$.

2.2. Calculation for $PM_{2.5}$ Concentration

All filters were weighed with an analytical balance (Sartorius, Germany) at least three times before and after sampling, following an equilibration for 48 h. The formula for mass concentration is shown as Eq. (1):

$$C = \frac{W_1 - W_0}{V_n} \times 10^6 \quad (1)$$

where C stands for $PM_{2.5}$ mass concentration ($\mu g/m^3$); W_0 and W_1 represent the weight before and after sampling, respectively (g); V_n represents the gas volume collected in a standard condition (m^3).

2.3. Analytical Method

Two haze days, November 4 (haze day 1, H1 sample) and December 24 (haze day 2, H2 sample) 2017 were selected for ions analysis, respectively. The sample from each day was analyzed for positive and negative ions by ToF-SIMS V (ION-ToF GmbH, Germany). The two working models of TOF-SIMS, i.e., static and dynamic, were applied to the samples. The static model was mainly for surface analysis (including surface mass spectrometry and image): 30 keV Bi^+ as primary ion beam, analysis area: $100 * 100$ um, 100 scans.[45] Dynamic model was mainly for depth profiling: 30 keV Bi^+ as primary ion beam, 10 keV Ar cluster as sputter beam, analysis area: $100 * 100$ um, sputter area: $500 * 500$ um, 300 scans for negative ions, 1000 scans for positive ions.

3. RESULTS AND DISCUSSION

3.1. Mass Concentration of $PM_{2.5}$

Figure 2 shows the variation of $PM_{2.5}$ mass concentration in Qiqihar for November and December (2016). The highest concentration was 183.1 $\mu g/m^3$ on November 4, and the lowest concentration was 19.1 $\mu g/m^3$ on December 22. The monthly mean concentration for November was 61.78 $\mu g/m^3$, which was lower than the mean value

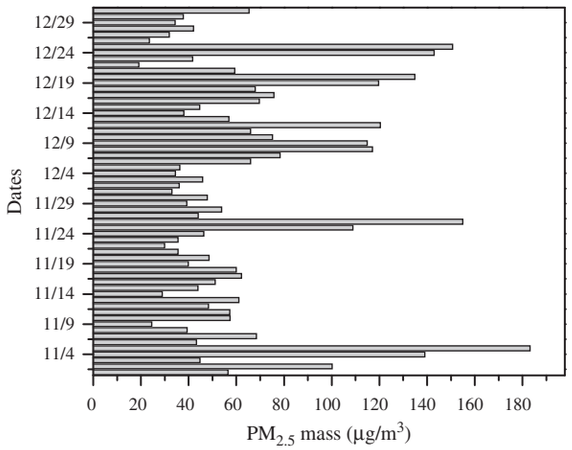

Fig. 2. The variation of $PM_{2.5}$ mass concentration.

of 67.08 $\mu g/m^3$ in December. In November and December the $PM_{2.5}$ concentrations were higher than the one in other months,[46] which may be related to various weather conditions and heating combustions.[47]

3.2. Secondary Image

For further comparing the ions distribution in the samples between November and December, the sample days, November 4th (H1 sample) and December 24th (H2 sample), were selected for each month, due to they had a similar mass concentration (Fig. 1).

The analysis results for ions distribution are shown in Figure 3. Although the two samples have a similar mass concentration, the ions distribution are very different. As showed, the brighter the image is, the stronger the response of secondary ions is. It is clear that the total positive ion response on H1 sample is stronger than that on H2 sample (Fig. 3(a)). The intensities of Na^+ and K^+ for the positive ions of H1 sample are significantly higher than those for H2 sample. The reason may be that the biomass combustion is enormously high in November; for instance, both crop straw and leaves burning makes K^+ increase significantly. However, the intensities of Ca^+ and Cu^+ in the positive ions of H2 sample are significantly higher than those in H1 sample. It may be related to the coal burning continuously in December. As shown in Figure 3(b), the intensity of each anion in H2 sample is also stronger than that in H1 sample, thus the brightness of the total anion for H2 sample is significantly stronger than the one for H1 sample, proving that the winter combustion source has a great influence on the air pollution in Qiqihar.

3.3. Mass Spectrometry Analysis on Surface Metal Ion

Both H1 and H2 samples were also analyzed for surface metal ions. The results were shown in Figures 4–6. It shows that K^+ was the strongest one, and the response value was 3.5×10^4, which is generally considered as an indicator of biomass combustion in inland cities,[48,49]

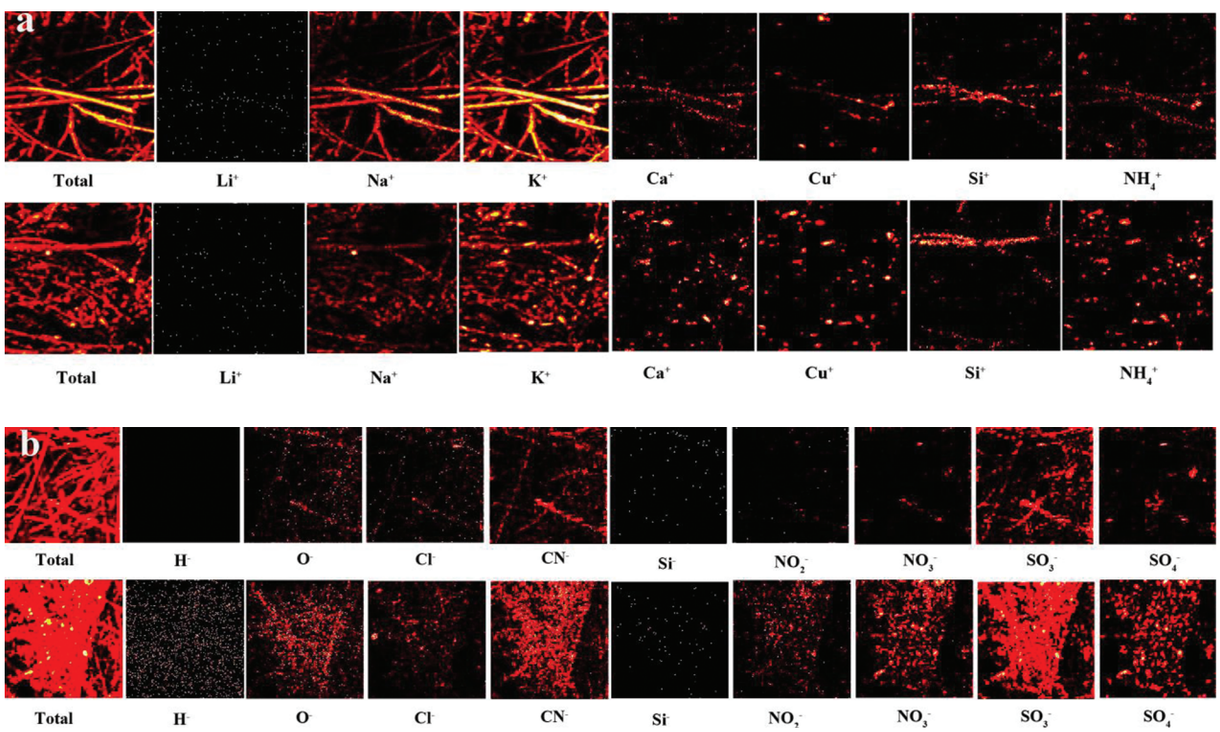

Fig. 3. Secondary ion images for H1 sample (the upper line of a and b) and H2 sample (the lower line of a and b). (a) Positive ions analysis; (b) negative ions analysis. Field of view: 100 $\mu m \times 100$ μm.

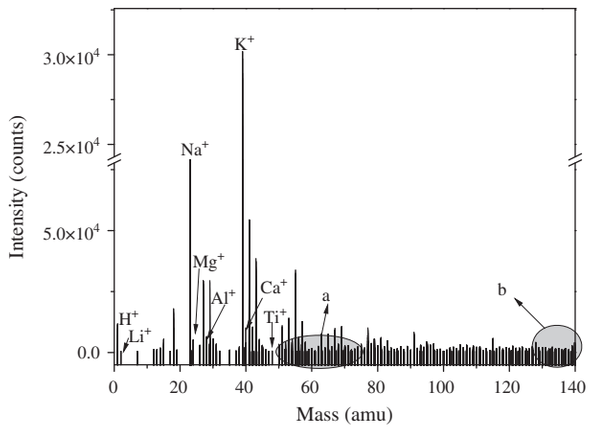

Fig. 4. The metal-ion ToF-SIMS spectra of $PM_{2.5}$ for H1. (a) of the figure is the Figure 5 and (b) of the figure is the Figure 6 (the results for H2 is similar).

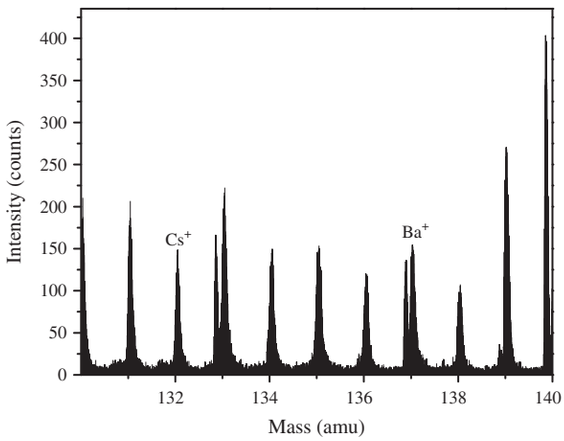

Fig. 6. The metal-ion ToF-SIMS spectra of $PM_{2.5}$ for H1 in the mass range of 130 to 140.

followed by Na^+ and Mg^+, and other metal ions such as Li^+, Al^+, Ca^+, Ti^+, Cr^+, Fe^+, Cu^+, As^+, Cs^+, Ba^+ and so on. The Na^+, Mg^+, Al^+, Si^+, Ca^+, Ti^+, and Fe^+ detected here are represented as mineral dusts, which mainly come from the source of crust.[50,51] The elements such as Cr^+, Fe^+, Cu^+ are mainly released from anthropogenic sources that include waste incineration, transport and industrial emission sources.[52] Other elements, such as As^+, Cs^+, and Ba^+, may come from the combination of natural and man-made pollution.[53] On the basis of these results, the pollution of $PM_{2.5}$ metal ions in Qiqihar originates from several sources, such as soil source, building source, coal source, traffic source and industrial emission. However, $PM_{2.5}$ was mainly derived from biomass combustion and fossil combustion in autumn and winter.

3.4. Depth Profiling

Depth profiling is a tool and can be used to analyze the variation of composition along with depth (sputter time).

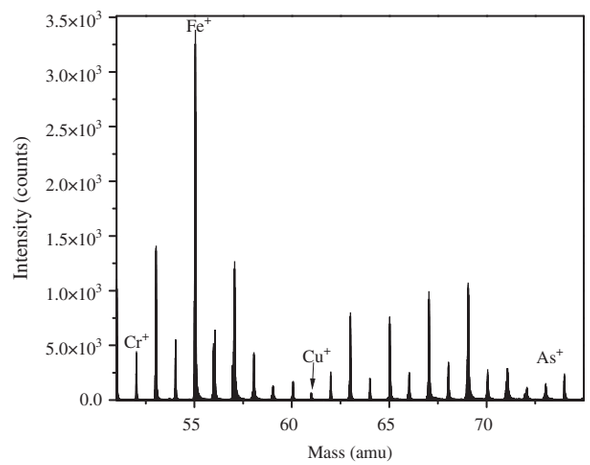

Fig. 5. The metal-ion ToF-SIMS spectra of $PM_{2.5}$ for H1 in the mass range of 50 to 75.

Although H1 and H2 samples have different response intensities for different ion species during the analysis of depth profiling, the trends for variation are the same. Therefore, only the H1 sample is selected for exhibition.

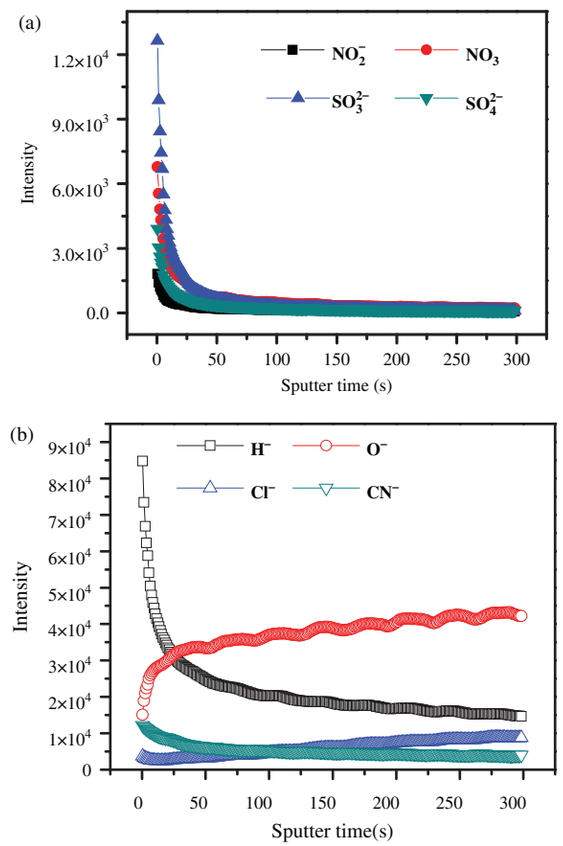

Fig. 7. TOF-SIMS depth profiles of $PM_{2.5}$ for H1 sample. Field of view: 100 μm × 100 μm, sputter area: 500 * 500 um, 300 scans for negative ions, (a and b): Negative ions; 1000 scans for positive ions. (The same analysis was performed for H2, but not show here, because the method is not a quantitative method).

ARTICLE

The results are shown in Figure 7. In Figure 7, the ordinate is the intensity, and the abscissa is sputter time. The longer the sputter time is, the greater the depth will be. As shown in Figure 7, the depth profiling for various inorganic ions is presented, where *a* and *b* are the analyses for negative ions, and *c* is the analysis for positive ions, *d* is for an ionic species of some inorganic salts and metal oxides. Along with the increase of sputtering time, the signal strength of negative ions (NO_2^-, NO_3^-, SO_3^{2-}, SO_4^{2-}) becomes weaker and weaker, and a constant value is reached when the sputtering time is over 50 s (Fig. 7(a)). The characteristics of secondary ions indicate that their active forms are mainly attached to the surface of $PM_{2.5}$. These surface secondary ions may react with other particles or chemicals, generating the harmness to human health. For instance, sulfur dioxide (SO_2) from exhaust gas of car can be oxidized in gaseous phase to form sulfur trioxide (SO_3), and then reacted with H_2O to form H_2SO_4. Afterwards, H_2SO_4 is condensed to the surface of particles to form sulfates.[54–56] The studies have shown that prolonged exposure to sulfur compounds can lead to respiratory and myocardial diseases.[57–63] On the other hand, the intensities of H^- and CN^- decreased along with the increase of sputtering time, and the intensities of O^- and Cl^- become stronger along with the increase of the depth (Fig. 7(b)). The mechanism for the phenomenon is not clear, but Laskin's research may provide some clues for an explanation. Laskin showed that NaCl particles could be wrapped by deliquescence products on the surface of the original particles. Once the surface reaction occurs, the Cl^- located on the surface would be exhausted,[64–69] but the Cl^- located inside the particles would not. This explains why the intensity of Cl^- will increase with increasing the depth. The intensities of K^+, Na^+ and NH_4^+ decreased along with the increase of sputtering time, the intensity of Na^+ reached a constant value after about 100 s sputtering (Fig. 8). Additionally, the intensities of ions, H^+, Al^+, Si^+ and Ca^+, increased along with the increase of the depth. However, the increase for H^+ and Al^+ is weaker, but the increase for Si^+ is stronger (Fig. 8). Interestingly, ion Ca^+

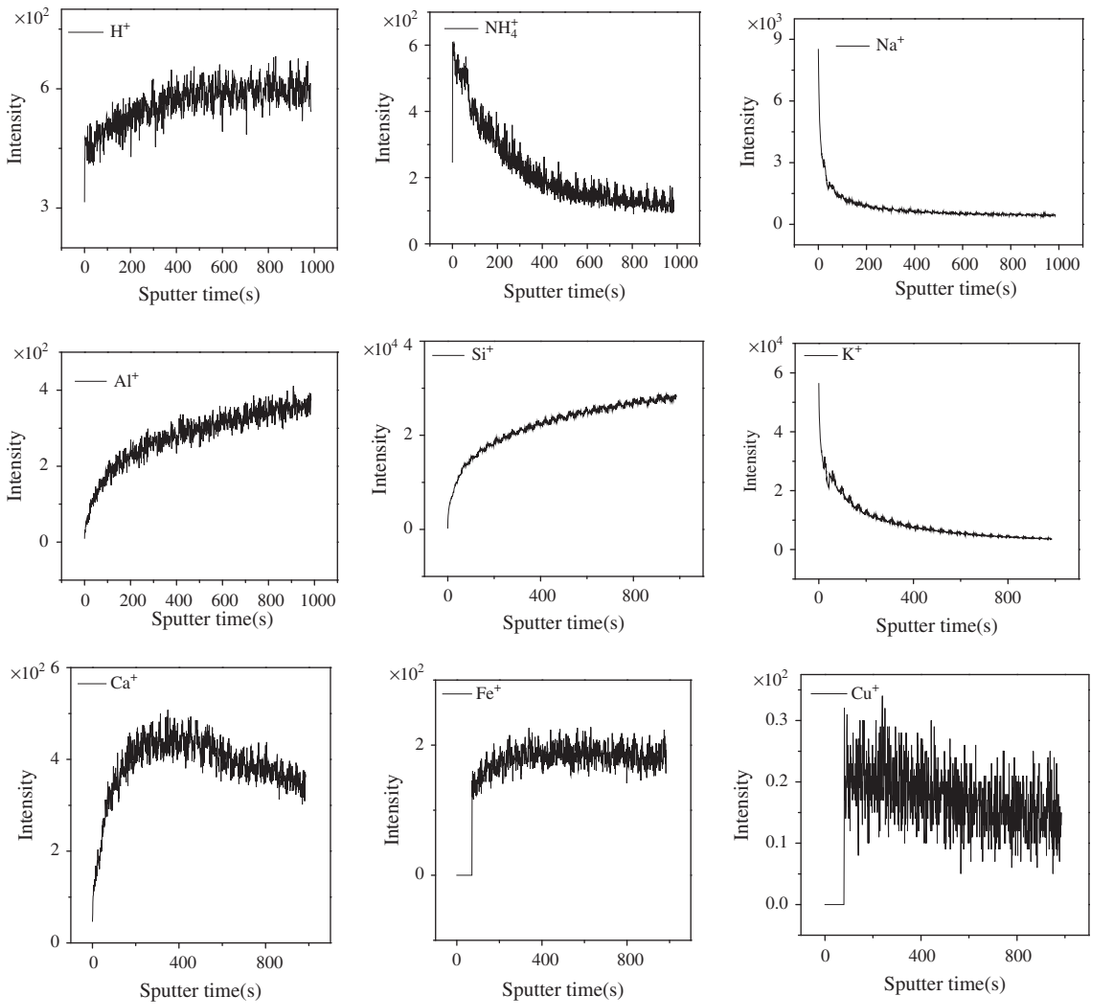

Fig. 8. TOF-SIMS depth profiles of $PM_{2.5}$ for H1 sample. Field of view: 100 μm × 100 μm, sputter area: 500∗500 um, 1000 scans for positive ions.

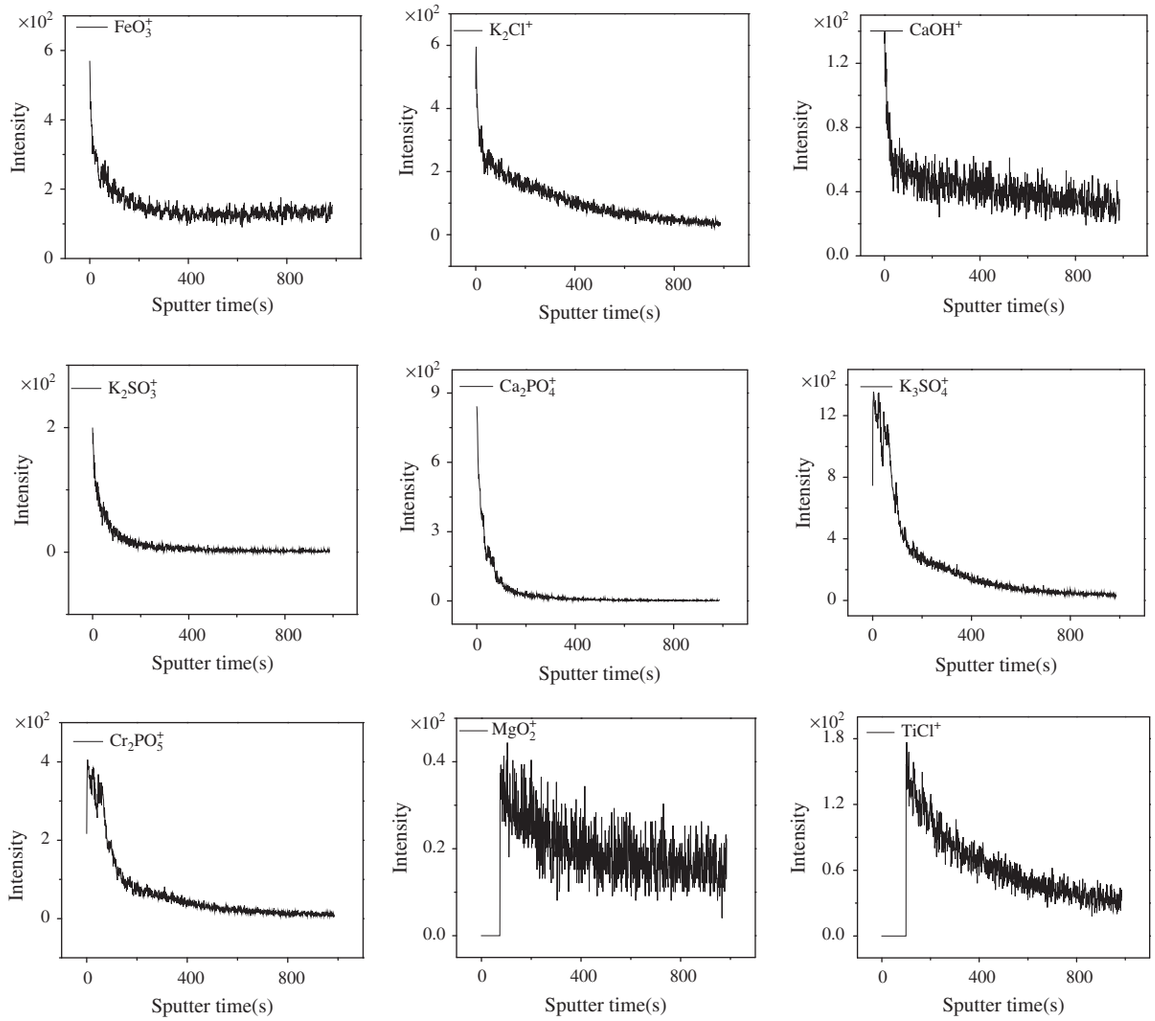

Fig. 9. TOF-SIMS depth profiles of $PM_{2.5}$ for H1 sample. Field of view: 100 μm × 100 μm, sputter area: 500 ∗ 500 um, 1000 scans for positive ions.

showed an increase first, and then decrease gradually. Fe^+ and Cu^+ did not show any response for first 100-second sputtering, after that, it began to show a response, meaning that the surface of the particles may be covered by other particles or they had reacted with other compositions to produce some other substances. The existence of inorganic salts and metal oxides on the surface of particles is showed in Figure 9. With the increase of sputtering time, the signal strength for these chemicals decreases, and then tends to be stable for short time. It means that the formation for these chemicals occurs on the surface of the particles. The results indicate that most of the inorganic particles are concentrated to the surface of the particles, and a few of them are buried inside of the particles.

4. CONCLUSION

Inorganic substances in $PM_{2.5}$ were characterized by TOF-SIMS in Qiqihar haze days, and the surface chemical composition information was obtained by secondary ion imaging and mass spectrometry, the changing trend on inorganic ions with depth is analyzed. The air pollution source in Qiqihar was addressed by tracing technique. The city of Qiqihar was seriously polluted in autumn and winter, and the pollution was mainly derived from biomass combustion and fossil combustion. Moreover, the biomass burning in autumn (November) is much more than that in winter (December), which means that biomass burning is more in November, but fossil combustion is more in December.

Acknowledgments: The authors are grateful for the Project supported by Qiqihar city industrial research project (QGG201309017).

References and Notes

1. C. Wang, B. Mo, Z. He, Q. Shao, D. Pan, E. Wujick, J. Guo, X. Xie, X. Xie, and Z. Guo, Crosslinked norbornene copolymer anion exchange membrane for fuel cells. *J. Membrane Sci.* 556, 118 (**2018**).

2. Z. Zhao, R. Guan, J. Zhang, Z. Zhao, and P. Bai, Effects of process parameters of semisolid stirring on microstructure of Mg–3Sn–1Mn–3SiC (wt%) strip processed by rheo-rolling. *Acta Metall. Sin. (Engl. Lett.)* 30, 66 **(2017)**.
3. Z. Zhao, P. Bai, R. Guan, V. Murugadoss, H. Liu, X. Wang, and Z. Guo, Microstructural evolution and mechanical strengthening mechanism of Mg–3Sn–1Mn–1La alloy after heat treatments. *Mater. Sci. Eng. A* 734, 200 **(2018)**.
4. Y. Zhao, L. Qi, Y. Jin, K. Wang, J. Tian, and P. Han, The structural, elastic, electronic properties and Debye temperature of D022-Ni3V under pressure from first-principles. *J. Alloys Compounds* 647, 1104 **(2015)**.
5. Y. Zhao, S. Deng, H. Liu, J. Zhang, Z. Guo, and H. Hou, First-principle investigation of pressure and temperature influence on structural, mechanical and thermodynamic properties of Ti3AC2 (A = Al and Si). *Comput. Mater. Sci.* 154, 365 **(2018)**.
6. B. Kirubasankar, V. Murugadoss, J. Lin, T. Ding, M. Dong, H. Liu, J. Zhang, T. Li, N. Wang, Z. Guo, and S. Angaiaha, *In-situ* grown nickel selenide onto graphene nanohybrid electrodes for high energy density asymmetric supercapacitors. *Nanoscale* 10, 20414 **(2018)**.
7. J. Guo, H. Song, H. Liu, C. Luo, Y. Ren, T. Ding, M. A. Khan, D. P. Young, X. Liu, X. Zhang, J. Kong, and Z. Guo, Polypyrrole-interface-functionalized nano-magnetite epoxy nanocomposites as electromagnetic wave absorber with enhanced flame retardancy. *J. Mater. Chem. C* 5, 5334 **(2017)**.
8. C. Cheng, R. Fan, Y. Ren, T. Ding, L. Qian, J. Guo, X. Li, L. An, Y. Lei, Y. Yin, and Z. Guo, Radio frequency negative permittivity in random carbon nanotubes/alumina nanocomposites. *Nanoscale* 9, 5779 **(2017)**.
9. C. Wang, Z. He, X. Xie, X. Mai, Y. Li, T. Li, M. Zhao, C. Yan, H. Liu, E. Wujcik, and Z. Guo, Controllable cross-linking anion exchange membranes with excellent mechanical and thermal properties. *Macromol. Mater. Eng.* 3, 1700462 **(2018)**.
10. C. Wang, B. Mo, Z. He, C. X. Zhao, L. Zhang, Q. Shao, X. Guo, E. Wujcik, and Z. Guo, Hydroxide ions transportation in polynorbornene anion exchange membrane. *Polymer* 138, 363 **(2018)**.
11. X. Cui, G. Zhu, Y. Pan, Q. Shao, C. Zhao, M. Dong, Y. Zhang, and Z. Guo, Polydimethylsiloxane-titania nanocomposite coating: Fabrication and corrosion resistance. *Polymer* 138, 203 **(2018)**.
12. Y. Zhang, M. Zhao, J. Zhang, Q. Shao, J. Li, H. Li, B. Lin, M. Yu, S. Chen, and Z. Guo, Excellent corrosion protection performance of epoxy composite coatings filled with silane functionalized silicon nitride. *J. Polym. Res.* 25, 130 **(2018)**.
13. H. Kang, Z.Cheng, H. Lai, H. Ma, Y. Liu, X. Mai, Y. Wang, Q. Shao, L. Xiang, X. Guo, and Z. Guo, Superlyophobic anti-corrosive and self-cleaning titania robust mesh membrane with enhanced oil/water separation. *Sep. Purif. Technol.* 201, 193 **(2018)**.
14. K. Gong, Q. Hu, L. Yao, M. Li, D. Sun, Q. Shao, B. Qiu, and Z. Guo, Ultrasonic pretreated sludge derived stable magnetic active carbon for Cr(VI) removal from wastewater. *ACS Sustain. Chem. Eng.* 6, 7283 **(2018)**.
15. S. Sun, L. Zhu, X. Liu, L. Wu, K. Dai, C. Liu, C. Shen, X. Guo, G. Zheng, and Z. Guo, Superhydrophobic shish-kebab membrane with self-cleaning and oil/water separation properties. *ACS Sustain. Chem. Eng.* 6, 9866 **(2018)**.
16. Z. Li, B. Wang, X. Qin, Y. Wang, C. Liu, Q. Shao, N. Wang, J. Zhang, Z. Wang, C. Shen, and Z. Guo, Superhydrophobic/superoleophilic polycarbonate/carbon nanotubes porous monolith for selective oil adsorption from water. *ACS Sustain. Chem. Eng.* 6, 13747 **(2018)**.
17. M. Dong, Q. Li, H. Liu, C. Liu, E. Wujcik, Q. Shao, T. Ding, X. Mai, C. Shen, and Z. Guo, Thermoplastic polyurethane-carbon black nanocomposite coating: Fabrication and solid particle erosion resistance. *Polymer* 158, 381 **(2018)**.
18. Z. Qu, M. Shi, H. Wu, Y. Liu, J. Jiang, and C. Yan, An efficient binder-free electrode with multiple carbonized channels wrapped by $NiCo_2O_4$ nanosheets for high-performance capacitive energy storage. *J. Power Sources* 410–411, 179 **(2019)**.
19. J. Huang, Y. Cao, Q. Shao, X. Peng, and Z. Guo, Magnetic nanocarbon adsorbents with enhanced hexavalent chromium removal: Morphology dependence of fibrillar versus particulate structures. *Ind. Eng. Chem. Res.* 56, 10689 **(2017)**.
20. Z. Zhao, H. An, J. Lin, M. Feng, V. Murugadoss, T. Ding, H. Liu, Q. Shao, X. Man, N. Wang, H. Gu, S. Angaiah, and Z. Guo, Progress on the photocatalytic reduction removal of chromium contamination. *Chem. Rec.* in press, DOI: 10.1002/tcr.201800153 **(2019)**.
21. J. Huang, Y. Li, Y. Cao, F. Peng, Y. Cao, Q. Shao, H. Liu, and Z. Guo, Hexavalent chromium removal over magnetic carbon nanoadsorbent: Synergistic effect of fluorine and nitrogen co-doping. *J. Mater. Chem. A* 6, 13062 **(2018)**.
22. K. Gong, S. Guo, Y. Zhao, Q. Hu, H. Liu, D. Sun, M. Li, B. Qiu, and Z. Guo, Bacteria cell templated porous polyaniline facilitated detoxification and recovery of hexavalent chromium. *J. Mater. Chem. A* 6, 16824 **(2018)**.
23. S. Weichenthal, E. Lavigne, G. Evans, K. Pollitt, and R. T. Burnett, Ambient $PM_{2.5}$ and risk of emergency room visits for myocardial infarction: Impact of regional $PM_{2.5}$ oxidative potential: A case-crossover study. *Environ. Health* 15, 46 **(2016)**.
24. Y. Xie, L. Bo, S. Jiang, Z. Tian, H. Kan, Y. Li, W. Song, and J. Zhao, Individual $PM_{2.5}$, exposure is associated with the impairment of cardiac autonomic modulation in general residents. *Environ. Sci. Pollut. R* 23, 10255 **(2016)**.
25. C. Feng, J. Li, W. Sun, Y. Zhang, and Q. Wang, Impact of ambient fine particulate matter ($PM_{2.5}$) exposure on the risk of influenza-like-illness: A time-series analysis in Beijing, China. *Environ. Health* 15, 17 **(2016)**.
26. F. Dominici, R. D. Peng, M. L. Bell, L. Pham, A. McDermott, S. L. Zeger, and J. M. Samet, Fine particulate air pollution and hospital admission for cardiovascular and respiratory diseases. *Jama-J. of the Am. Med. Assoc.* 295, 1127 **(2006)**.
27. K. Xu, C. Liu, K. Kang, Z. Zheng, and S. Wang, Isolation of nanocrystalline cellulose from rice straw and preparation of its biocomposites with chitosan: Physicochemical characterization and evaluation of interfacial compatibility. *Compos. Sci. Technol.* 154, 8 **(2018)**.
28. Y. Lim, H. Kim, J. Kim, S. Bae, H. Park, and Y. Hong, Air pollution and symptoms of depression in elderly adults. *Environ. Health Persp.* 120, 1023 **(2012)**.
29. R. D. Brook, Cardiovascular effects of air pollution. *Clin. Sci.* 115, 175 **(2008)**.
30. H. Gnaser, Focused ion beam implantation of Ga in InP studied by SIMS and dynamic computer simulations. *Surf. Interface Anal.* 43, 28 **(2011)**.
31. D. Myers, Surface, Interface, and Colloids: Principles and Applications, Chemical Industry Press **(2005)**, pp.243–258.
32. D. C. Blanchard, The ejection of drops from the sea and their enrichment with bacteria and other materials: A review. *Estuar. Coast.* 12, 127 **(1989)**.
33. S. Wang and T. Zhu, The research progress of source apportionment of airborne particulate matter. *Techniques and Equipment for Environmental Pollution Control* 3, 8 **(2002)**.
34. L. Paoletti, B. D. Berardis, L. Arrizza, M. Passacantando, M. Inglessis, and M. Mosca, Seasonal effects on the physico-chemical characteristics of PM2.1 in Rome: A study by SEM, and XPS. *Atmos. Environ.* 37, 4869 **(2003)**.
35. L. T. González, F. E. L. Rodríguez, M. S. Domínguez, M. C. L. Porras, L. G. S. Vidaurri, K. A. Askar, B. I. Kharisov, J. F. V. Chiu, and J. M. A. Barbosa, Chemical and morphological characterization of TSP and $PM_{2.5}$, by SEM-EDS, XPS and XRD collected in the metropolitan area of Monterrey, Mexico. *Atmos. Environ.* 143, 249 **(2016)**.
36. R. R. Leal, M. V. Martinez, and M. C. Campas, Elemental analysis of particles $PM_{2.5}$ by SEM-EDS. *Microsc. Microanal.* 22, 2058 **(2016)**.

ARTICLE

37. D. Roy, G. Singh, and N. Gosai, Identification of possible sources of atmospheric PM_{10} using particle size, SEM-EDS and XRD analysis, Jharia Coalfield Dhanbad, India. *Environ. Monit. Assess.* 187, 1 **(2015)**.

38. Y. Zhu, N. Olson, and T. P. Beebe, Surface chemical characterization of 2.5-microm particulates ($PM_{2.5}$) from air pollution in salt lake city using TOF-SIMS, XPS, and FTIR. *Environ. Sci. Technol.* 35, 3113 **(2001)**.

39. J. Goschnick, M. Fichtner, M. Lipp, J. Schuricht, and H. J. Ache, Depth-resolved chemical analysis of environmental microparticles by secondary mass spectrometry. *Appl. Surf. Sci.* 70–71, 63 **(1993)**.

40. J. Goschnick and J. Schuricht, Surface and depth analysis of pollen treated with atmospheric trace gases. *J. Aerosol Sci.* 27, 229 **(1996)**.

41. N. Klaus, Sims analysis of aerosols collected during a weather period with low aerosol concentrations. *Sci. Total Environ.* 41, 1 **(1985)**.

42. N. Klaus, The configuration of impactor deposits analyzed by secondary ion mass spectroscopy. *Sci. Total Environ.* 37, 187 **(1984)**.

43. R. E. Peterson and B. J. Tyler, Analysis of organic and inorganic species on the surface of atmospheric aerosol using time-of-flight secondary ion mass spectrometry (TOF-SIMS). *Atmos. Environ.* 36, 6041 **(2002)**.

44. A. Benninghoven and L. Cha, TOF-SIMS—A powerful tool for practical surface, interface and thin film analysis. *Vacuum* **(2002)**.

45. D. Huang, G. Xiu, M. Li, X. Hua, and Y. Long, Surface components of $PM_{2.5}$, during clear and hazy days in Shanghai by ToF-SIMS. *Atmos. Environ.* 148, 175 **(2017)**.

46. J. Tian, J. Lv, and Y. Zheng, Determination and sources analysis of water-soluble ions in atmosphere environment $PM_{2.5}$ of qiqihar city. *Bull. Sci. Technol.* 8, 221 **(2016)**.

47. G. Liu, Atmospheric Environmental Monitoring, Meteorological Press, Beijing, China (in Chinese) **(2012)**, pp. 9–29.

48. M. O. Andreae, Soot carbon and excess fine potassium: Long-range transport of combustion-derived aerosols. *Science* 220, 1148 **(1983)**.

49. B. R. T. Simoneit, J. J. Schauer, C. G. Nolte, D. R. Oros, V. O. Elias, M. P. Fraser, W. F. Rogge, and G. R. Cass, Levoglucosan, a tracer for cellulose in biomass burning and atmospheric particles. *Atmos. Environ.* 33, 173 **(1999)**.

50. R. A. Duce, C. K. Unni, B. J. Ray, J. M. Prospero, and J. T. Merrill, Long-range atmospherictransport of soil dust from Asia to the tropical North Pacific: Temporal variability. *Science* 209, 1522 **(1980)**.

51. S. R. Taylor and S. M. Mclennan, The Continental Crust: Its Composition and Evolution, An Examination of the Geochemical Record Preserved in Sedimentary Rocks, Blackwell Scientific Pub. **(1985)**.

52. K. Adachi and Y. Tainosho, Characterization of heavy metal particles embedded in tire dust. *Environ. Inter.* 30, 1009 **(2004)**.

53. T. Okuda, M. Katsuno, D. Naoi, S. Nakao, S. Tanaka, K. He, Y. Ma, Y. Lei, and Y. Jia, Trends in hazardous trace metal concentrations in aerosols collected in Beijing, China from 2001 to 2006. *Chemosphere* 72, 917 **(2008)**.

54. H. Saathoff, K. H. Naumann, M. Schnaiter, W. Schöck, O. Möhler, U. Schurath, E. Weingartner, M. Gysel, and U. Baltensperger, Coating of soot and $(NH_4)_2SO_4$ particles by ozonolysis products of alpha-pinene. *J. Aerosol Sci.* 34, 1297 **(2003)**.

55. K. S. Johnson, B. Zuberi, L. T. Molina, M. J. Molina, M. J. Iedema, J. P. Cowin, D. J. Gaspar, C. Wang, and A. Laskin, Processing of soot in an urban environment: Case study from the mexico city metropolitan area. *Atmos. Chem. Phys.* 5, 3033 **(2005)**.

56. J. H. Seinfeld and S. N. Pandis, Atmospheric Chemistry and Physics: From Air Pollution to Climate Change, Wiley **(2012)**.

57. F. W. Lipfert, Sulfur Oxides, Particulates, and Human Mortality: Synopsis of Statistical Correlations. *J. Air Poll. Control Association* 30, 366 **(1980)**.

58. D. P. Rall, Review of the health effects of sulfur oxides. *Environ. Health Persp.* 8, 97 **(1974)**.

59. M. H. Brown and D. H. Deyoung, Three-stage process for burning fuel containing sulfur to reduce emission of particulates and sulfur-containing gases, U.S. Patent 4542704 **(1985)**.

60. T. M. Chen, W. G. Kuschner, J. Gokhale, and S. Shofer, Outdoor air pollution: Nitrogen dioxide, sulfur dioxide, and carbon monoxide health effects. *Am. J. Med. Sci.* 333, 249 **(2007)**.

61. H. Jin, A. Liu, L. Holmberg, M. Zhao, S. Chen, J. Yang, Y. Sun, S. Chen, C. Tang, and J. Du, The role of sulfur dioxide in the regulation of mitochondrion-related cardiomyocyte apoptosis in rats with isopropylarterenol-induced myocardial injury. *Int. J. Mol. Sci.* 14, 10465 **(2013)**.

62. B. G. Ferris Jr., F. E. Speizer, J. D. Spengler, D. Dockery, Y. M. M. Bishop, M. Wolfson, and C. Humble, Effects of sulfur oxides and respirable particles on human health methodology and demography of populations in study. *Am. Rev. Resp. Dise.* 120, 767 **(1979)**.

63. J. H. Ware, L. A. Thibodeau, F. E. Speizer, S. Colome, and B. G. Ferris Jr., Assessment of the health effects of atmospheric sulfur oxides and particulate matter: Evidence from observational studies. *Environ. Health Persp.* 41, 255 **(1981)**.

64. A. Laskin, D. J. Gaspar, W. Wang, S. W. Hunt, J. P. Cowin, S. D. Colson, and B. J. Finlayson-Pitts, Reactions at interfaces as a source of sulfate formation in sea-salt particles. *Science* 301, 340 **(2003)**.

65. R. C. Hoffman, A. Laskin, and B. J. Finlayson-Pitts, Sodium nitrate particles: Physical and chemical properties during hydration and dehydration, and implications for aged sea salt aerosols. *J. Aerosol Sci.* 35, 869 **(2004)**.

66. A. Laskin, R. C. Moffet, M. K. Gilles, J. D. Fast, R. A. Zaveri, B. Wang, P. Nigge, and J. Shutthanandan, Tropospheric chemistry of internally mixed sea salt and organic particles: Surprising reactivity of NaCl with weak organic acids. *J. Geophys. Res.-Atmos.* 117, 156 **(2012)**.

67. A. Laskin, J. Laskin, and S. A. Nizkorodov, Mass spectrometric approaches for chemical characterisation of atmospheric aerosols: Critical review of the most recent advances. *Environ. Chem.* 9, 163 **(2012)**.

68. A. Laskin, M. K. Gilles, D. A. Knopf, B. Wang, and S. China, Progress in the analysis of complex atmospheric particles. *Annu. Rev. Anal. Chem.* 9, 117 **(2016)**.

69. Y. Sheng, J. Yang, F. Wang, L. Liu, H. Liu, C. Yan, and Z. Guo, Sol–gel synthesized hexagonal boron nitride/titania nanocomposites with enhanced photocatalytic activity. *Appl. Surface Sci.* 465, 154 **(2019)**.

ARTICLE